https://doi.org/10.1016/j.jmst.2021.06.067

High-temperature mechanical behavior of ultra-coarse cemented carbide with grain strengthening

Huaxin Hu [a], Xuemei Liu[a,*], Jinghong Chen [a], Hao Lu[a], Chao Liu[b], Haibin Wang [a], Junhua Luan[c], Zengbao Jiao[d], Yong Liu[e], Xiaoyan Song [a,*]

[a] *Faculty of Materials and Manufacturing, Key Laboratory of Advanced Functional Materials, Ministry of Education of China, Beijing University of Technology, Beijing 100124, China*

[b] *Xiamen Tungsten Co., Ltd., Xiamen 361009, China*

[c] *Department of Materials Science and Engineering, City University of Hong Kong, Hong Kong, China*

[d] *Department of Mechanical Engineering, The Hong Kong Polytechnic University, Hong Kong, China*

[e] *State Key Laboratory of Powder Metallurgy, Central South University, Changsha 410083, China*

Abstract

Ultra-coarse grained cemented carbides are often used under conditions of concurrently applied stress and high temperature. Improvement of high-temperature mechanical performance of ultra-coarse grained cemented carbides is highly desirable but still a big challenge. In this study, it is proposed that the high- temperature compression strength of ultra-coarse cemented carbides can be enhanced by modulating hard matrix grains by activated TaC nanoparticles, through solid solution strengthening of Ta atoms. Based on the designed experiments and microstructural characterizations combined with finite element simu- lations, the grain morphology, stress distribution

and dislocation configuration were studied in detail for ultra-coarse grained cemented carbides. The mechanisms of Ta dissolving in WC crystal and strengthen- ing ultra-coarse grains through interaction with dislocations were disclosed from the atomic scale. This study opens a new perspective to modulate hard phases of cemented carbides for improving their high- temperature performance, which will be applicable to a variety of cermet and ceramic-based composite materials.

1. Introduction

Cemented carbides are typical composites consisting of hard matrix and metallic binder. This kind of materials possesses high hardness and excellent wear resistance thus fulfills many engineering requirements. The ultra-coarse grained WC-Co cemented carbides, which normally have WC grain sizes larger than 5 μm, can offer properties with a good combination of hardness and fracture toughness. Therefore, it is widely used in coal mining, rock drilling, tunneling and pavement maintenance [1–3]. Because of the harsh working conditions, the ultra-coarse grained cemented carbides have to be capable to bear contact and cyclic loads, severe mechanical and thermal fatigue with abrupt temperature variations, which brings a great challenge to the service life of this kind of materials [4–6]. To extend their service life, further increase in the fracture strength especially at elevated temperatures is highly demanded for ultra-coarse grained WC-Co cemented carbides [7–9].

For cemented carbides, the metallic binder plays a critical role in coordinating the plastic deformation of the material, especially at the initial stage of deformation. The

WC skeleton is significant to the mechanical properties of the cemented carbides on the whole, as it is the matrix and has a much higher volume fraction than that of binder. As reported in a latest research [10], the calculated energy stored in WC grains was obviously higher than that in Co binder when the ultra-coarse grained cemented carbides were compressed at different temperatures, from which it was proposed that the WC phase may have larger contribution to the plastic deformation of the cemented carbides than Co binder. Though the WC skeleton exists as a hard matrix in cemented carbides to mainly provide the hardness and strength for the material, it can still become soft at high temperatures. Luca et al. investigated the properties of individual phases in cemented carbides from ambient to high temperature [11], and found that deformation of WC in both prismatic and basal planes could be thermally activated, and the fracture of WC grains started at a temperature of 500°C. Basically, ultra-coarse grained cemented carbides have much smaller volume fraction of grain and phase boundaries and lower intragranular strength compared with fine-grained cemented carbides[12,13]. Therefore, the most effective route to improve the mechanical performance of ultra-coarse WC-Co cemented carbides at both room and high temperatures is to strengthen the large WC grains.

For the fine grained cemented carbides, it has been reported in the literature that various grain growth inhibitors (GGIs), most of which are carbides of refractory metals, were added in the ini- tial powders to control grain growth during sintering densification. However, many GGIs exist in the sintered cemented carbides in forms of complexions or precipitates at WC grain boundaries or WC/Co interfaces, or partially dissolve in Co

binder [14]. It was found that the refractory metals in the GGIs, such as V [15–18], Cr [19–21], and Ti [22,23], tend to form refractory-metal-riched layers at WC/WC grain boundaries thus inhibit the grain growth [24–28]. Very few GGI has been found to be dissolved in WC grains.

It was reported in the previous work that addition of TaC resulted in the formation of a brittle honeycombed (W,Ta) C cubic phase at the interfaces [29–32]. When the TaC content was more than 0.6wt.%, both the strength and fracture toughness of the cemented carbides were reduced due to the formation of brit- tle (W,Ta) C [30]. For high-temperature tests, the hardness of TaCcontaining cemented carbides slowly increased due to the compe- tition between WC grain refinement and the formation of (W,Ta) C brittle clusters [31]. Ostberg et al. found that Ta had different ef- fects on the mechanical properties in the bending test of cemented carbides at different temperatures [32]. The addition of TaC can strengthen the carbide skeleton by harder (W,Ta) C phase, while the formation of (W,Ta) C may result in easier sliding or infiltration of grain boundaries at high temperatures due to its poor wettabil- ity with Co.

Actually, the effects of TaC addition on the mechanical performance of cemented carbides have not been deeply understood. It is considered by the authors that the contribution of Ta to the mechanical properties of cemented carbides mainly depends on the existing form and location of TaC or Ta. For this, experiments were designed in this work to investigate the effects of pre-treated TaC on the microstructure and mechanical properties of ultra-coarse grained cemented carbides at high temperatures.

2. Experimental

2.1 Material preparation

The tungsten carbide powder with a mean particle size of ~22.2μm and a mean grain size of ~8.6μm, Co powder with a mean particle size of ~2.0 μm, WC-Co composite powder with a mean particle size of ~100 nm, and pre-milled (activated) TaC powder with a mean particle size of 80nm were used as raw materials. The activated TaC powder was prepared by the high energy milling process, which was conducted in the highly pure Ar atmo- sphere to minimize contaminations. The purpose of refining the TaC was to enhance the activity of the powder and improve the dissolution capacity of the TaC particles during the sintering pro- cess. The milling process was continued for 36h (with half an hour cooling every 1.5h) with a ball to powder mass ratio of 60:1 and a rotation speed of 500 r/min. To focus on the deformation char- acteristics of the hard phase, a relatively low Co content of 8 wt.% was used. The WC-8Co and WC-8Co-0.8TaC powder mixtures were prepared by ball milling with a rotation speed of 350 r/min. For the goal of a same level of grain size in the cemented carbide samples, longer time was applied to the milling process of WC-8Co powder while shorter milling time was used for the WC-8Co-0.8TaC pow- der. After optimization of experiments, the WC-8Co-0.8TaC powder was milled for 5 h and the WC-8Co powder was milled for 6.5 h, respectively. Then the milled powders were both sintered in Ar at- mosphere at 1480 °C under a pressure of 60 bar for 80 min.

The sintered bulk materials were electro-discharge machined into cylinder

samples with dimensions of mm. The cylinder samples underwent uniaxial compression for the high-temperature performance tests operated by Thermemcmastor, with the testing temperatures set as 600, 800, and 1000°C at a strain rate of 0.5 .

2.2 Characterization

The microstructure of the samples was observed by the scanning electron microscope (SEM, JSM 6500). The electron back scattered diffraction (EBSD) analysis was performed using the EDAX TSL Hikari EBSD detector with a scanning step of 400 nm. Based on the EBSD results, the dislocation density of WC grains at different compression temperatures were calculated by the method reported in the literature [33–37].

As proposed in the literature, the dislocation density is proportional to the misorientation angle between the neighboring WC grains. Therefore, the dislocation density of WC grains at different compression temperatures can be calculated from the Kernel average misorientation (KAM) obtained by EBSD. The dislocation density can be estimated by the following formula:

$$\rho = \frac{2v}{ub}$$

where μ is the unit length, b is the magnitude of the Burgers vector and v is the misorientation angle. As a first order approach, the KAM was chosen as a measure for the local misorientations. It quantifies the average misorientation around a measurement point with respect to a defined set of nearest or nearest plus second-nearest neighbor points. Values above a predefined threshold (here it is 2°) are excluded

from the calculation.

The dislocations were also examined by the transmission electron microscope (TEM) and high-resolution TEM (HRTEM) operated at 200kV (JEM-2100F). The energy dispersive spectroscopy (EDS) maps were acquired via high-angle annular dark-field (HAADF) imaging in an aberration-corrected scanning transmission electron microscope (STEM). Needle-shaped specimens required for atom probe tomography (APT) were fabricated by lift-outs and annular milled in a FEI Scios focused ion beam/scanning electron micro- scope (FIB/SEM). The APT characterizations were performed in a local electrode atom probe (CAMECA LEAP 5000 XR).

The stress distribution in the microstructure of the cemented carbide after 800°C compression was obtained by finite element simulation. In the simulations, the dimension of the models was 82.8×82.8 μm2 including more than 100WC grains. The compression simulation was carried out by applying a compressive load of 1000MPa. The material properties derived and extrapolated from the data reported in the literature [44–47] were used in this study. The temperature effect was introduced into the parameter, as shown in Table 1.

3. Results

3.1 Effect of TaC on microstructure characteristics

Fig. 1 shows the microstructures and the corresponding grain size distributions of the WC phase in the as-sintered WC-8Co and WC-8Co-0.8TaC cemented carbide specimens. From the comparison of the grain morphology in Fig. 1(a) and (b), it is

worth noting that the specimen with TaC addition has more rounded edges of WC grains near the WC/Co phase boundary, as indicated by the white arrows. It is conjectured that the addition of TaC may influence the dissolution-precipitation processes of W and C atoms in the liquid Co during sintering, hence influence the morphology of coarse WC grains locally at WC/Co phase boundaries. Because of this partially rounded shape of WC grains, the probability of contact between the sharp corners of WC is reduced. Correspondingly, the contiguity of WC decreases from 0.6 to 0.53 by the addition of TaC ob- tained by stereological analysis for Fig. 1. The mean free path of Co decreases from 2.70 to 2.45 μm after adding TaC, indicating that the WC and Co phase distributions are more uniform. No segregation of brittle (W,Ta) C phase is observed from the backscattered electron image of the specimen with TaC addition Fig. 1(b). By adjusting the processing parameters (see 'Experimental section'), the grain sizes of the specimens with and without TaC addition are very close (~6.30 μm in Fig. 1(a) and ~6.27μm in Fig. 1(b)). The grain size distributions (shown in the inserted plots) are narrow in both specimens. Under the condition that the specimens have very close mean grain size and similar grain size distribution, the compression tests are considered to reflect only the effect of composition (instead of grain size) on the mechanical behavior of the ultra-coarse grained cemented carbides.

3.2 Compressive performance at high temperatures

3.2.1Compressive strength

As shown in Fig. 2, the compressive strength of the specimens decrease

continuously with the increase of temperature in the range of 600–1000°C, and the strength of the specimens with TaC addition are higher than those of the specimens without TaC at each temperature. The contiguity of WC grains, measured by the stereological method, is shown in the insert of Fig. 2 for the specimens after compressed at different temperatures. It shows a trend of decrease with the increase of temperature, indicating the Co film squeezing into the WC grain boundaries during high temperature compression process, which was also demonstrated by the molecular dynamics simulation [48]. The lower contiguity of WC in the WC-8Co-0.8TaC specimen is favorable to release local stress concentration, which normally exists at contacting areas of WC grains. Despite the creep of Co phase is more serious, the WC-8Co-0.8TaC specimens still have a higher compressive strength than WC-8Co, which implies the inhibition on the plastic deforma- tion of WC phase due to the TaC addition.

3.2.2 Crack density

Fig.3 shows the crack density on the polished surface at the fracture topography of specimens after compression. The cracks were statistically analyzed for more than 100 cracks. As the compression temperature was increased from 600 to 1000°C, the crack density decreased in both specimens. Interestingly, no matter what the compression temperature is, the crack density in WC-8Co specimen is at least 16% higher than that of WC-8Co-0.8TaC specimen. The crack density in the WC-8Co specimen compressed at 800°C is estimated to be 4.59 × 103 m−1, which is about 1.3 times higher than that in the WC-8Co-0.8TaC specimen (3.51 × 103 m−1). The statistical analysis on cracks implies that adding TaC can reduce the crack density when

the cemented carbide is severely deformed.

Generally, the location of stress concentration can be the source of crack initiation, which may even cause the failure of materials. Therefore, to examine the stress distribution under hightemperature compression is necessary and indispensable to analyze the crack initiation. Here the finite element method was used to construct models based on the real microstructures of WC-8Co and WC-8Co-0.8TaC specimens at 800°C. The results shown in Fig.4(a) and (b) indicate that both the specimens have an inhomo- geneous stress distribution: there is a low stress level in Co phase, but a high level stress at WC skeleton. The stress distributions in the WC skeletons of the WC-8Co and WC-8Co-0.8TaC specimens after compression at 800°C are shown in Fig.4(c). At the WC skele- ton with similar morphology, the specimen with TaC addition has lower stress compared to the WC-8Co counterpart. In detail, the stress values of the WC-8Co-0.8TaC is reduced about 24% at the triple junction, 23% at the grain boundary, and 17% at the corner of WC grains than the counterpart of WC-8Co at 800 °C. The lower stress state in WC-8Co-0.8TaC is mainly caused by the formation of round-shaped WC grains and the decrease in the contiguity of WC. This implies that TaC addition is beneficial to reduce the stress concentration at the WC skeleton, therefore impedes the initiation of microcracks at the WC grain boundaries and triple junctions. Therefore, there are less cracks occurred in the WC-8Co-0.8TaC specimen, which is consist with the analysis of crack density in Fig. 3.

3.2.3 Dislocation analysis

The dislocation density of WC grains at different compression temperatures were calculated based on the KAM obtained by EBSD. To ensure the accuracy of the dislocation density results, more than 350 grains were selected for statistical counting. Fig.5 shows the average dislocation density of WC and the dislocation density distribution on the (0001) plane of WC grains in the WC-8Co and WC-8Co-0.8TaC specimens compressed at different temperatures.

As seen in Fig. 5, the dislocation density in WC grains of the WC-8Co-0.8TaC specimen is always higher than the counterpart with no addition at all the temperatures. In both specimens, the change of the average dislocation density of WC grains exhibits a non-monotonic trend with the increase of temperature. As the temperature increases from 600 to 800 °C, the dislocation density increases, which may be attributed to that more types of slip sys- tems are activated and the energy barriers for the motion of different dislocations become similar at higher temperature [38]. While as the compression temperature increases further to 1000°C, the dislocation density in WC decreases. The main reason is that the recovery of dislocations at higher temperature is more activated, leading to fewer dislocations pilled-up in WC grains. Another reason is that, grain boundary sliding (GBS) is the main deformation mechanism at higher temperatures that can accommodate the applied stress [39,40], leading to fewer dislocations generated in WC grains at 1000°C.

In general, slip mainly occurs on the prismatic and pyramidal planes regardless of

room temperature or high temperature for WC crystals with a hexagonal close packed (hcp) structure [38,41]. According to the crystallographic characteristics of WC crystals, most dislocation lines on the basal plane (0001) are slip traces of the dislocations which slip on the prismatic or pyramidal planes. Therefore, the dislocation lines on the basal plane can reflect the active dislocations in the main slip systems of WC crystals. Comparing the dislocation density distributions on the basal plane (0001) of a single WC grain, it confirms that the dislocation den- sity in the specimen with TaC addition is higher than that of the specimen without TaC at each compression temperature, which is consist with the comparison on the average dislocation density in WC for the two kinds of specimens. It gave a hint that in the WC- 8Co-0.8TaC specimen, there may exist foreign atoms, clusters, or precipitates in the WC crystal, which hinder the motion of disloca- tions inside the WC grains, and inhibit the recovery of dislocations at high temperatures. Thus, there is a higher WC dislocation den- sity in the specimens with TaC addition.

As proposed in the literature [38,41,49], the active slip systems of WC grains are mainly in the prismatic planes, and the dislocations in the basal plane are active at high temperatures. Therefore, to investigate the difference in the dislocation characteristics of the two kinds of cemented carbide specimens, the dislocations were observed from two representative directions, i.e. along the normal directions of basal plane (0001) and prismatic plane ($1\bar{2}1\bar{0}$), pectively. In order to find out the effect of TaC on the WC dislocations, the field of view was selected from the region in the vicinity of the round edge of WC grains in the WC-8Co-TaC specimen. As shown in Fig. 6, dramatic

differences can be observed between the dislocation configurations of the two kinds of specimens. The WC-8Co specimen has the typical pattern of planar slip with long and straight dislocation lines Fig. 6(a and b), while the WC-8Co-0.8TaC specimen has a multidirectional dislocation network with a high population of corrugated and short dislocation lines Fig. 6(c) and (d). Similar pattern with that in WC-8Co-0.8TaC is referred to ‘wavy slip’ in literature [42]. Crystallographic analysis shows that the dislocations are primarily on prismatic planes in both specimens. The dislocation lines are relatively straight in the WC-8Co specimen, and the dislocations are nearly aligned. In contrast, dis- location lines in the WC-8Co-0.8TaC specimen exhibit an obvious stagnated state or a kinked characteristic, indicating the occurrence of local pinning or cross-slip onto adjacent crystal planes. In the WC-8Co specimen, most dislocations lie in planes parallel to prismatic plane and form a large number of stacking faults, also they interact with short dislocations parallel to (0001), , or planes. In contrast, the dislocations in the WC- 8Co-0.8TaC specimen do not show such planarity, the dislocations mainly parallel to prismatic planes are curved, creating a relatively homogeneous distribution in the WC grain.

3.2.4 Element distribution

From the above results, it is confirmed that the differences in the compressive behavior and microstructure of the ultra-coarse grained cemented carbides are generated by the addition of TaC. To disclose the existing form and distribution of the added TaC, the composition in the vicinity of phase boundary with round edge of WC grain in the WC-8Co-0.8TaC specimen was examined. The composition distribution

and the element contents along the line across the phase boundary are shown in Fig.7. The bright and dark regions in the HAADF image in Fig.7(a) correspond to WC grain and Co binder, respectively. From the elemental distri- butions in Fig.7(b–e), it suggests a homogeneous distribution of Ta in the observed WC region, and a small amount of W and C atoms are dissolved in the Co phase. Moreover, as shown in Fig.7(f), the line scan analysis confirms that Ta has a high solubility in the local zone of WC grain, but little exists in the Co phase.

Three-dimensional atom probe (3DAP) technique was used to further analyze the distribution of Ta atoms, and the analyzed positions are marked by white circles in the SEM image in Fig. 8. In the center of WC grain Fig. 8(a), only W and C atoms are observed. In the Co phase, a small amount of W and C atoms are detected Fig. 8(b), which indicates that WC can be partly dissolved in Co in the liquid-state sintering process. Inside the WC grain, in the position close to the WC/Co boundary, except for W and C, Ta atoms are observed in a concentrated state Fig. 8(c).

From Figs.6–8, combining the results obtained by STEM-EDS and 3DAP, as well as the selected area electron diffraction, it can be summarized that Ta element is more likely to distribute in WC grains in a form of solid solution atoms, instead of segregating in Co phase or at WC/Co boundaries.

4. Discussion

In this section, the mechanisms of Ta dissolution in WC and the interaction between Ta atoms with WC dislocations which strengthens the hard WC grain will be

discussed.

4.1 Ta dissolution in WC crystal

Fig. 9 reveals the evolution of the microstructure of the ultracoarse grained cemented carbide with TaC addition during the sintering process, and the corresponding schematic diagrams illustrate the processes of Ta dissolving into WC grains. During the mixing procedure, the WC-Co composite nanoparticles facilitate the dispersion of TaC nanoparticles, and a homogeneous distribution of nanoscale TaC and WC-Co composite powders and microscale WC particles can be obtained Fig.9(a1 and a2). Rapid WC grain growth may occur during the solid-state sintering stage, as shown in Fig.9(b1) and (b2), which is caused by the large driving force from high surface energy of nanoscale particles. In this coarsening process, there is a re-distribution of TaC, i.e., between the locations in WC grains and at WC/Co interfaces Fig.9(b2). With the temperature increasing to the liquid-state sintering stage, Ta, W, and C atoms can dissolve into liquid Co. Ta atoms can further diffuse into WC during the dissolution-precipitation processes, as shown by “A” in Fig.9(c2). Inside the WC crystal, interdiffusion of Ta and W atoms may occur, as demonstrated in “B” in Fig.9(c2).

Based on the experimental detection on the composition, combined with the above analysis, it is inferred that Ta distributes in WC grains in a range from tens to hundreds of nanometers from the WC/Co phase boundary. With an atomic radius of 2.09 , which is slightly larger than W atomic radius of 2.02 [43], Ta atoms prefer to occupy W sites in the WC lattice to form a substitutional solid solution (Fig. 9d).

According to the above analysis, using the WC-Co composite nanoparticles with appropriate carbon content in the raw powder mixture is beneficial to the uniform distribution of the TaC nanoparticles, hence the formation of a WC based solid solution with Ta atoms, which prevents the formation of the (W,Ta) C phase during dissolution and precipitation in the sintering process.

4.2 Interaction between dissolved Ta and WC dislocations

It is observed in Fig. 6 that, there are dramatically different dislocation configurations in WC-8Co and WC-8Co-0.8TaC specimens. Take the typical dislocation on the prismatic plane as an example (corresponding to Fig. 6a and c), Fig. 10 illustrates the in- teraction between Ta and WC dislocations. In a WC crystal without TaC addition, the dislocations on the prismatic plane slip along the direction of , and then move towards the interface (Fig. 10a). Therefore, the typical WC dislocations are straight when extending in the grains. In contrast, in the WC grain containing Ta as substitutional solute atoms, the lattice distortion and discrete pinning points caused by Ta atoms may interact with the moving dislocations during the deformation process. The motion of dislo- cations in the slip system will be hindered, which results in local bow-out of dislocations, as shown in Fig. 10(b). Moreover, Ta-rich clusters may form in the WC crystal, which can inhibit dislocation movement more strongly. As a result, WC dis- locations will tend to cross-slip onto adjacent prismatic planes or basal planes, as shown in Fig. 10(c) and (d). Consequently, the dislocation configuration in the WC-8Co-0.8TaC specimen exhibits a form of multidirectional dislocation network with a high population of corrugated and short

dislocation lines. As analyzed above, the strengthening of Ta to the WC grains results in the increase of strength of the WC-8Co-0.8TaC specimen.

5. Conclusion

In the present work, the effect of TaC addition on the high- temperature compressive behavior of the ultra-coarse grained cemented carbides was studied by analyzing the grain morphology, stress distribution, and dislocation configuration. The relationship between the compressive strength, WC contiguity, and dislocation configuration with the temperature and TaC addition have been established. Based on a series of experimental characterizations and stress calculations, the strengthening mechanisms for the ultra-coarse grained cemented carbides by Ta dissolving into WC were proposed. The main conclusions are drawn as follows.

（1）The WC grains in the ultra-coarse cemented carbide with TaC addition have a low contiguity and a characteristic morphology with round edges at the WC/Co phase boundaries. At the same level of ultra-coarse grain size, the cemented carbide with TaC has obviously increased compressive strength at high temperatures compared with the counterpart with no addition.

（2）The stress concentration in the WC skeleton (particularly at triple junctions, grain boundaries, and corners) is reduced due to TaC effect on grain shape and contiguity. The WC dislocation density in the cemented carbide with TaC is always higher than that in the counterpart with no addition at all the temperatures, indicating less recovery occurred in the WC grain.

（3）Ta distribution in WC grains with round edges was identified by atomic composition detection. The strengthening mechanisms were proposed for the ultra-coarse cemented carbide with TaC based on the demonstration of interactions between WC dislocations and substitutional Ta solute atoms and resultant lattice distortion. This also explains for the specific wavy slip of dislocations due to Ta dissolution in WC.

Declaration of Competing Interest

The authors declare no conflict of interest.

Acknowledgments

This work was supported by the National Key Program of Re- search and Development (No. 2018YFB0703902) and the National Natural Science Foundation of China (Nos. 51631002, 51621003,52101003, 52171061, U20A20236).

References

[1] U. Beste, S. Jacobson, Wear 264 (2008) 1129–1141.

[2]X. Ren, H. Miao, Z. Peng, Int. J. Refract. Met. Hard Mater. 39 (2013) 61–77.

[3]P.K. Katiyar, Int. J. Refract. Met. Hard Mater. 92 (2020) 105315.

[4]L. Llanes, Y. Torres, M. Anglada, Acta Mater. 50 (2002) 2381–2393.

[5]I. Konyashin, F. Lachmann, B. Ries, A.A. Mazilkin, B.B. Straumal, C. Kübel, L. Llanes, B. Baretzky, Scr. Mater. 83 (2014) 17–20.

[6]J. Heinrichs, M. Olsson, S. Jacobson, Int. J. Refract. Met. Hard Mater. 64 (2017) 7–

13.

[7]H.G. Schmid, D. Mari, W. Benoit, C. Bonjour, Mater. Sci. Eng. A 105–106 (1988) 343–351.

[8]D. Jianxin, Z. Hui, W. Ze, L. Yunsong, Z. Jun, Int. J. Refract. Met. Hard Mater. 31 (2012) 196–204.

[9]Y. Lu, J. Tang, Z. Ge, B. Xia, Y. Liu, Int. J. Rock Mech. Min. Sci. 60 (2013) 47–56.

[10]X. Liu, C. Hou, H. Lu, H. Hu, H. Wang, X. Song, Int. J. Refract. Met. Hard Mater. 88 (2020) 105177.

[11]F. De Luca, H. Zhang, K. Mingard, M. Stewart, B.M. Jablon, C. Trager-Cowan, M.G. Gee, Materialia 12 (2020) 100713.

[12]H. Wang, M. Gee, Q. Qiu, H. Zhang, X. Liu, H. Nie, X. Song, Z. Nie, J. Mater. Sci. Technol. 35 (2019) 2435–2446.

[13]A. Vornberger, J. Pötschke, T. Gestrich, M. Herrmann, A. Michaelis, Int. J. Refract. Met. Hard Mater. 88 (2020) 105170.

[14]X. Liu, X. Song, H. Wang, X. Liu, F. Tang, H. Lu, Acta Mater. 149 (2018) 164–178.

[15]S. Lay, S. Hamar-Thibault, A. Lackner, Int. J. Refract. Met. Hard Mater. 20 (2002) 61–69.

[16]I. Sugiyama, Y. Mizumukai, T. Taniuchi, K. Okada, F. Shirase, T. Tanase, Y.

Ikuhara, T. Yamamoto, Scr. Mater. 69 (2013) 473–476.

[17]M. Kawakami, K. Kitamura, Int. J. Refract. Met. Hard Mater. 52 (2015) 229–234.

[18]H. Chen, Q. Yang, J. Yang, H. Yang, L. Chen, J. Ruan, Q. Huang, J. Alloys Compd. 714 (2017) 245–250.

[19]A. Delanoë, M. Bacia, E. Pauty, S. Lay, C.H. Allibert, J. Cryst. Growth 270 (2004) 219–227.

[20]W. Guo, K. Li, Y. Du, Z. Zhang, T. Xu, C. Yin, Z. Zhang, P. Zhou, X. Liu, B. Huang, Int. J. Refract. Met. Hard Mater. 58 (2016) 68–73.

[21]S. Lay, A. Antoni-Zdziobek, J. Pötschke, M. Herrmann, Int. J. Refract. Met. Hard Mater. 93 (2020) 105340.

[22]S. Lay, M. Loubradou, W.D. Schubert, J. Am. Ceram. Soc. 89 (2006) 3229–3234.

[23]J. Weidow, H.O. Andrén, Int. J. Refract. Met. Hard Mater. 29 (2011) 38–43.

[24]J. Weidow, H.O. Andrén, Acta Mater. 58 (2010) 3888–3894.

[25]M. Christensen, G. Wahnström, Acta Mater. 52 (2004) 2199–2207.

[26]M. Christensen, G. Wahnström, Int. J. Refract. Met. Hard Mater. 24 (2006) 80–88.

[27]S.A.E. Johansson, G. Wahnström, Acta Mater. 59 (2011) 171–181.

[28]J. Weidow, H.O. Andrén, Ultramicroscopy 111 (2011) 595–599.

[29]N. Li, W. Zhang, Y. Du, W. Xie, G. Wen, S. Wang, Scr. Mater. 100 (2015) 48–50.

[30]W. Su, Y.X. Sun, H.L. Yang, X.Q. Zhang, J.M. Ruan, Trans. Nonferr. Met. Soc. China 25 (2015) 1194–1199.

[31]W. Su, Y. Sun, H. Yang, X. Zhang, J. Ruan, Effects of TaC on microstructure and mechanical properties of coarse grained WC9Co cemented carbides[J]. Trans. Nonferr. Met. Soc. China 25 (2015) 1194–1199.

[32]G. Östberg, K. Buss, M. Christensen, S. Norgren, H.O. Andrén, D. Mari, G. Wahnström, I. Reineck, Int. J. Refract. Met. Hard Mater. 24 (2006) 145–154.

[33]M. Calcagnotto, D. Ponge, E. Demir, D. Raabe, Mater. Sci. Eng. A 527 (2010) 2738–2746.

[34]J. Jiang, T.B. Britton, A.J. Wilkinson, Acta Mater. 61 (2013) 7227–7239.

[35]S. Birosca, G. Liu, R. Ding, J. Jiang, T. Simm, C. Deen, M. Whittaker, Int. J. Plast. 118 (2019) 252–268.

[36]B. Jiao, Q. Zhao, Y. Zhao, L. Li, Z. Hu, X. Gao, W. Zhang, J. Li, J. Mater. Sci. Tech- nol. 92 (2021) 208–213.

[37]J. Luo, H. Luo, T. Zhao, R. Wang, J. Mater. Sci. Technol. 93 (2021) 128–146.

[38]H. Hu, X. Liu, C. Hou, H. Wang, F. Tang, X. Song, Acta Crystallogr. Sect. B Struct. Sci. Cryst. Eng. Mater. 75 (2019) 1014–1023.

[39]G. Östberg, K. Buss, M. Christensen, S. Norgren, H.O. Andrén, D. Mari, G. Wahn-

ström, I. Reineck, Int. J. Refract. Met. Hard Mater. 24 (2006) 135–144.

[40]X. Han, N. Sacks, Y.V. Milman, S. Luyckx, Int. J. Refract. Met. Hard Mater. 27 (2009) 274–281.

[41]M. Bľanda, A. Duszová, T. Csanádi, P. Hvizdoš, F. Lofaj, J. Dusza, J. Eur. Ceram. Soc. 34 (2014) 3407–3412.

[42]S. Zhao, R. Zhang, Y. Chong, X. Li, A. Abu-Odeh, E. Rothchild, D.C. Chrzan, M. Asta, J.W. Morris, A.M. Minor, Nat. Mater. 20 (2021) 468–472.

[43]K. Barbalace, Periodic Table of Elements, EnvironmentalChemistry.com, 2021 1995.

[44]H.D. Merchant, G.S. Murty, S.N. Bahadur, L.T. Dwivedi, Y. Mehrotra, J. Mater. Sci. 8 (1973) 437–442.

[45]V. Livescu, B. Clausen, J.W. Paggett, A.D. Krawitz, E.F. Drake, M.A.M. Bourke, Mater. Sci. Eng. A 399 (2005) 134–140.

[46]V.T. Golovchan, Int. J. Refract. Met. Hard Mater. 25 (2007) 341–344.

[47]Z. Huang, Y. He, H. Cai, Y. Xiao, B. Huang, Trans. Nonferr. Met. Soc. China 18 (2008) 660–664.

[48]J. Fang, X. Liu, H. Lu, X. Liu, X. Song, Acta Crystallogr. Sect. B Struct. Sci. Cryst. Eng. Mater. 75 (2019) 134–142.

[49]X. Liu, J. Zhang, C. Hou, H. Wang, X. Song, Z. Nie, Mater. Des. 150 (2018) 154–164.

Table 1 Plastic properties of Co and elastic properties of WC and Co at 800°C.

Material	Young's modulus (GPa)	Poisson's ratio	Yield stress (MPa)	Hardening modulus (GPa)
WC	548.5	0.19	-	-
Co	174	0.31	549	52.4

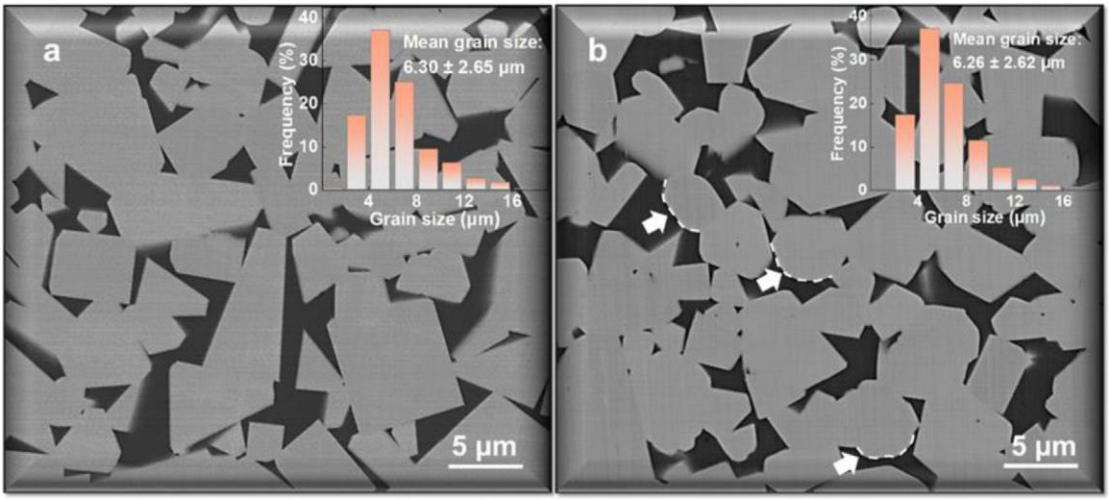

Fig. 1. Backscattered electron images of microstructures of as-sintered (a) WC-8Co and (b) WC-8Co-0.8TaC ultra-coarse cemented carbides, with rounded edges of WC grains marked by white arrows. Inset: the corresponding WC grain size distributions.

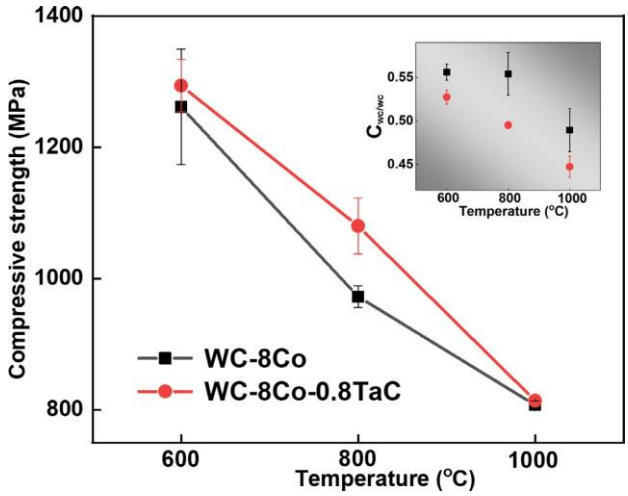

Fig. 2. Compressive strength of WC-8Co and WC-8Co-0.8TaC specimens at different temperatures. The insert shows the WC contiguity in the specimens at different compression temperatures.

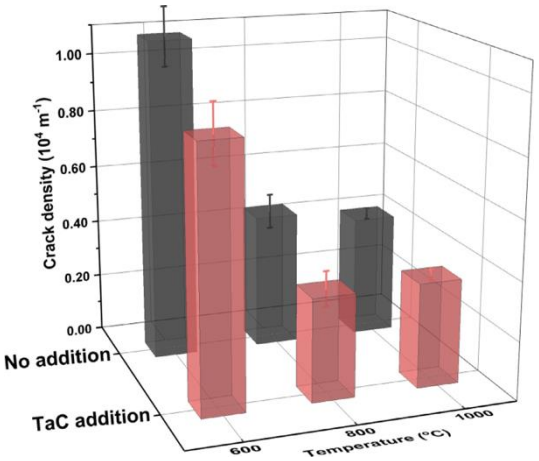

Fig 3. Statistical analysis of crack density at different temperatures for WC-8Co and WC-8Co-0.8TaC specimens.

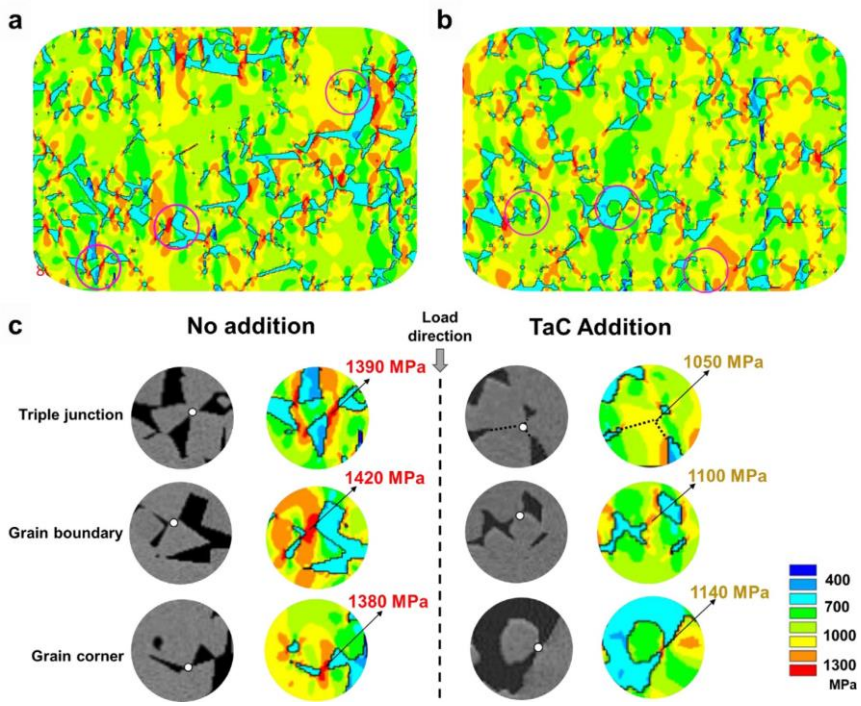

Fig. 4. Stress distributions in the microstructures of WC-8Co (a) and WC-8Co-0.8TaC(b) specimens after compression at 800°C, and comparison of the stress distribution at representative locations at WC skeleton between WC-8Co (left panel) and WC-8Co-0.8TaC (right panel) specimens (c). The local regions in (c) are corresponding to those circled in (a) and (b), respectively.

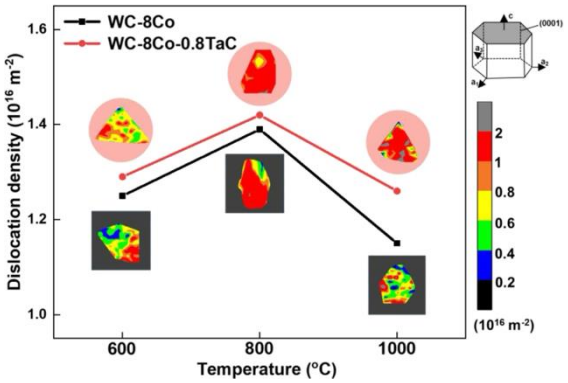

Fig. 5. Average dislocation density in WC grains and the dislocation density at (0001) WC plane in WC-8Co and WC-8Co-0.8TaC specimens compressed at different temperatures

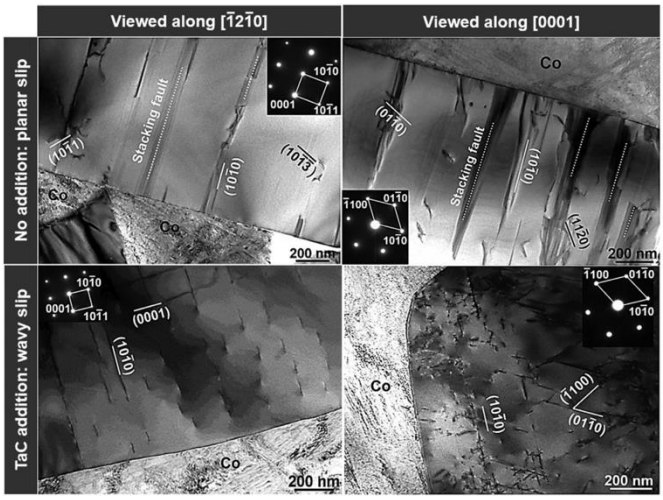

Fig.6. Dislocations in WC-8Co(a, b) and WC-8Co-0.8TaC(c, d) specimens after compression at 800°C, observed along $[\bar{1}2\bar{1}0]$ and [0001] directions, respectively.

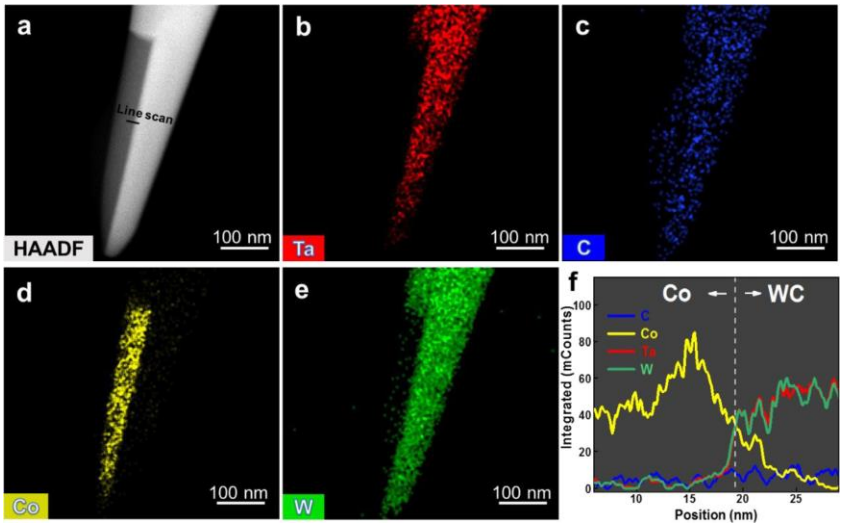

Fig. 7. Composition analysis in the vicinity of WC/Co phase boundary with round edge of WC grain in the WC-8Co-0.8TaC specimen: (a) HAADF image of a phase boundary; (b–e) Elemental distributions of Ta, C, Co, and W in the vicinity of phase boundary; (f) Composition distribution along the line marked in (a).

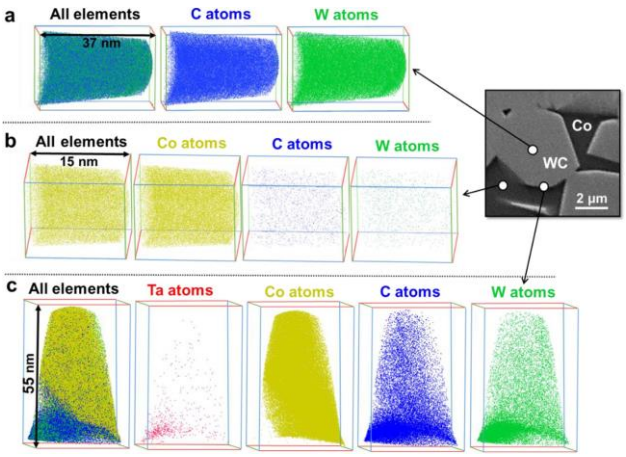

Fig. 8. 3DAP analysis on the position in WC grain (a), Co phase (b), and at WC/Co phase boundary (c) in the WC-8Co-0.8TaC specimen. The analyzed positions are marked by white circles in the SEM image.

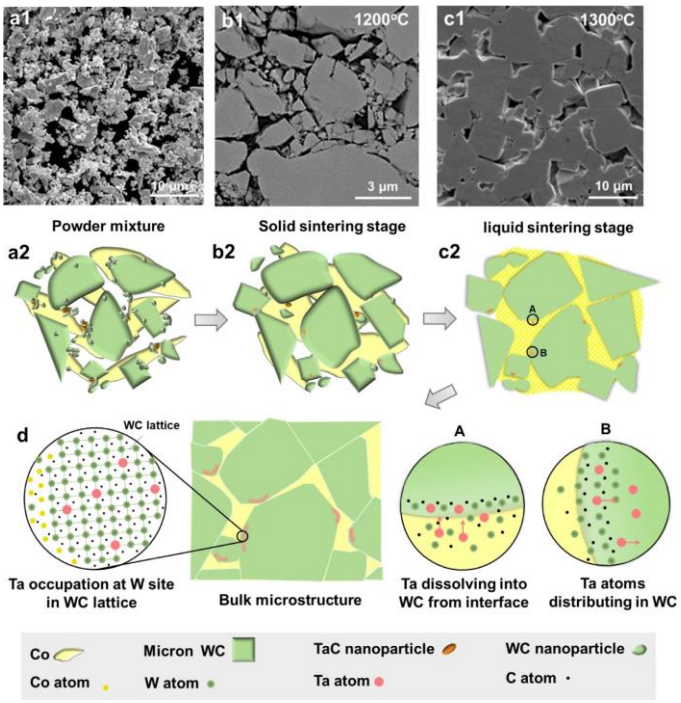

Fig. 9. Microstructure evolution of the ultra-coarse grained cemented carbide with TaC addition during sintering, and schematic diagrams illustrating the processes of Ta dissolving into WC grains: (a1, a2) Mixing of powder particles; (b1, b2) Solid-state sintering stage, where rapid WC grain growth occurs; (c1,c2) Liquid-state sintering stage, where Ta diffuses into WC during the dissolution-precipitation processes; (d) Ta distribution in WC lattice by occupying *W* sites.

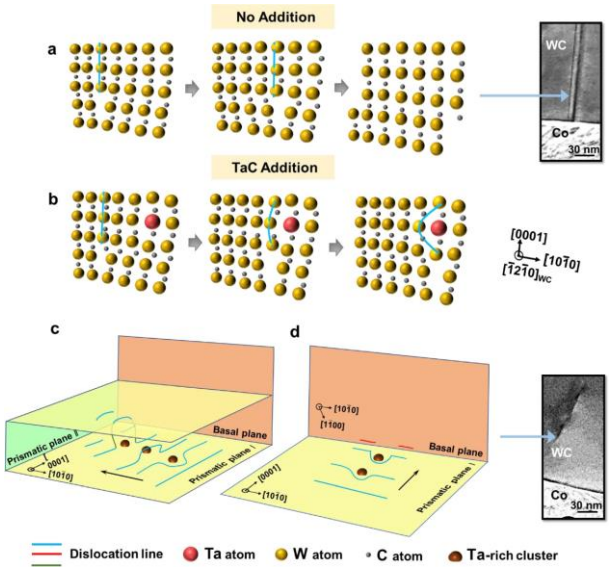

Fig.10. Schematic diagrams for the formation of WC dislocation patterns: (a) Typical dislocations slip in WC crystal without any addition; (b) Dislocations slip in WC crystal containing substitutional Ta solute atoms; (c, d) Cross-slip of WC dislocations onto adjacent prismatic and basal planes, respectively, when hindered by Ta-rich clusters, leading to the formation of corrugated and short dislocation lines on the slip plane.